Teknomekanik, Vol. 9, No. 2, 2026, pp. 218-237
e-ISSN: 2621-8720 p-ISSN: 2621-9980

Flow-rate estimation in PVC and carbon-steel pipes using flow-induced vibrations and data-driven models

Khalid Alnabhani[1], Musaab Zarog[2*], and Hadj Bourdoucen[3]

[1] Department of Mechanical and Industrial Engineering, College of Engineering, University of Technology and Applied Sciences, **Sultanate of Oman**
[2] Department of Mechanical and Industrial Engineering, College of Engineering, Sultan Qaboos University, **Sultanate of Oman**
[3] Department of Electrical and Computer Engineering, College of Engineering, Sultan Qaboos University, **Sultanate of Oman**

[*]Corresponding Author: musaabh@squ.edu.om
Received: 07 January 2026; *Revised:* 26 April 2026; *Accepted:* 07 May 2026

Cite this https://doi.org/10.24036/teknomekanik.v9i2.53072

Abstract: Non-intrusive flow measurement methods are increasingly required in pipeline systems to eliminate pressure losses, prevent contamination, and avoid structural modifications. Flow-induced vibration (FIV) offers a promising alternative; however, its applicability to standard industrial carbon-steel pipelines and its integration with data-driven modeling remain limited. This study experimentally investigates FIV-based flow estimation in 1-inch PVC and carbon-steel pipes conveying water under controlled conditions using regression, and machine learning models, while examining the influence of pipe material and vibration-response characteristics on flow-rate prediction performance. Vibration responses were measured using a tri-axial accelerometer and analyzed to identify flow-sensitive frequency bands. Regression and machine-learning models were developed to relate vibration characteristics to flow rate. The results demonstrate a predominantly monotonic relationship between band-averaged vibration amplitude and flow rate, with material-dependent sensitivity observed between PVC and carbon-steel pipes. Data-driven models improved prediction performance and robustness on the dynamic behavior of flow-induced vibrations, The findings demonstrate the potential of combining FIV analysis with intelligent modeling as a non-intrusive approach for flow measurement in industrial pipelines. Neural time-series modeling was used for training purpose only. Open-loop training provides a stable and efficient way for the network to learn the underlying dynamic relationship between inputs and outputs. A meaningful assessment of the model's predictive capability requires closed-loop testing, where the network relies on its own previous predictions. This was not conducted in the present study.

Keywords: frequency-domain analysis; flow-induced vibrations; machine learning; neural network; non-intrusive flow measurement

1. Introduction

Accurate flow-rate measurement is essential in civil and industrial pipeline systems for process control, safety, operational reliability, and energy efficiency [1]. Flow monitoring plays a critical role in various applications, including water distribution networks, oil and gas transportation, chemical processing, and thermal systems, where inaccurate measurements can lead to operational inefficiency, increased energy consumption, and safety risks [2]. In many industrial applications, conventional intrusive flow meters may disturb the flow field, introduce pressure losses, increase maintenance requirements, and suffer from fouling or sensor degradation over long-term operation. Consequently, non-intrusive flow measurement techniques have gained increasing attention because they enable flow monitoring without direct contact with the fluid, thereby

reducing contamination risk, installation complexity, operational downtime, and maintenance costs [3], [4], [5].

Flow-induced vibrations (FIV) in pipes arise from the interaction between turbulent fluid flow and the structural response of the pipe. As the flow rate increases, the fluid velocity and Reynolds number rise, leading to turbulence characterized by unsteady velocity fluctuations. The instantaneous velocity can be expressed as $u = \bar{u} + u'$, where $\bar{u}$ is the mean velocity, and u' represents the fluctuating component. These fluctuations generate Reynolds stresses, which contribute to wall shear stress and pressure variations within the flow field [6]. The resulting pressure fluctuations act as dynamic excitation forces on the pipe wall and induce structural vibration through fluid structure interaction mechanisms [7], [8]. From a structural perspective, the pipe can be modeled as a beam subjected to distributed pressure loading. According to beam theory, the relationship between pressure fluctuations and structural response can be expressed as $EI\frac{d^4y}{dx^4} = p'(x)$, where E is Young's modulus, I is the second moment of area, and y is the transverse deflection. This indicates that fluctuating internal pressure directly induces pipe deformation and vibration, particularly in the transverse direction where structural compliance is higher [9], [10]. This fluid-structure interaction provides the physical basis for using vibration measurements as a non-intrusive method for flow-rate estimation.

Several experimental studies have demonstrated a strong relationship between flow-rate and flow-induced vibration (FIV) response using different sensing techniques and analysis strategies. Accelerometer-based investigations commonly employ frequency-domain analysis, in which vibration amplitudes are extracted within selected frequency regions, and have reported a predominantly linear increase with flow rate under specific operating conditions [11], [12], [13], [14]. Similar frequency-based approaches have been applied using a Laser Doppler vibrometer (LDV), confirming comparable trends [15], [16]. In contrast, other accelerometer-based studies have utilized time-domain statistical features, such as the standard deviation of vibration signals, and reported a quadratic relationship with flow rate, particularly at higher Reynolds numbers [10], [17], [18]. Likewise, distributed acoustic sensing (DAS) techniques rely on phase variation analysis, representing another time-domain-based strategy, and have also demonstrated strong nonlinear relationships between flow-rate and turbulence-induced fluctuations [19], [20]. These observations indicate that the extracted relationship is strongly dependent on the selected signal representation and analysis strategy.

In addition to the signal processing strategy, pipe material and geometry significantly influence the vibration response. Comparative studies using PVC, stainless steel, and aluminum pipes have shown that flexible materials such as PVC produce higher vibration amplitudes due to lower stiffness, while stiffer materials such as stainless steel yield weaker responses, with aluminum exhibiting intermediate behavior [10], [16]. Large-eddy simulation (LES) studies further support these material-dependent trends [13]. Similarly, geometric parameters such as pipe diameter and wall thickness significantly influence the dynamic response and vibration transmission characteristics of fluid-conveying pipes [21]. Larger diameters and thicker walls generally reduce vibration amplitudes by increasing structural stiffness and reducing sensitivity to turbulent excitation forces [22], [23]. These findings highlight that the measured vibration signal is governed by a coupled fluid-structure interaction rather than fluid behavior alone.

Recently, machine-learning and artificial intelligence techniques have gained increasing attention in vibration-based monitoring and diagnostic systems because of their ability to extract complex patterns from nonlinear vibration signals and improve monitoring accuracy under varying operating conditions. In structural health monitoring applications, deep learning and vibration-based data analysis techniques have been widely used for damage detection, crack identification, and structural condition assessment [24], [25]. In industrial machinery systems, vibration-based machine-learning

methods have also demonstrated strong capability for fault diagnosis and early detection of mechanical degradation using advanced signal-processing approaches [26]. In addition, artificial intelligence techniques integrated with distributed sensing and vibration-monitoring systems have been explored for leakage detection and continuous condition monitoring applications in pipeline systems [20], [27]. Furthermore, recent studies have investigated data-driven approaches for predicting dynamic responses and flow-induced vibration behavior under turbulent operating conditions [28].

Despite these advances, several limitations remain in the current literature. Many studies rely on a single analysis strategy, either frequency-domain amplitude extraction or time-domain statistical features, without systematically comparing their effectiveness. In addition, the integration of advanced data-driven approaches, capable of capturing the nonlinear and dynamic characteristics of FIV, has not been comprehensively explored, particularly for industrial carbon-steel pipelines under controlled turbulent flow conditions. Accordingly, the objective of this work is to evaluate both physics-based and data-driven approaches for flow-rate estimation from FIV signals, thereby improving the reliability and applicability of non-intrusive flow-monitoring techniques for industrial pipelines.

These gaps highlight the need for a unified framework that systematically compares different signal representations and analysis strategies while accounting for material and geometric effects. This motivates the present study, which first establishes the flow-vibration relationship using physically meaningful, flow-sensitive frequency features identified through Strouhal-based estimation. This step provides a physics-based understanding of how vibration characteristics relate to flow rate. The analysis is then extended to data-driven modeling, where classical machine-learning approaches are applied using different input representations, including time-domain signals, full-spectrum frequency data, and band-limited features. This integrated approach allows both physical interpretation and model-based prediction, improving the robustness and generalizability of non-intrusive flow-rate estimation.

2. Material and methods

An experimental investigation was conducted using a closed-loop flow facility designed to study (FIV). The setup enables controlled variation of flow rate and measurement of hydraulic and structural response variables under repeatable operating conditions.

2.1 Closed-loop flow facility

The flow rig shown in Figure 1 consists of a storage reservoir, a centrifugal pump, a main circulation pipeline, flow control components, and a dedicated test section. The closed-loop configuration ensures continuous circulation of the working fluid and stable operation over a wide range of flow rates. The reservoir has a total capacity of approximately 400 L and supplies the working fluid to the system. Fluid circulation is driven by a centrifugal pump rated at 3 hp. The main pipeline is constructed from 2-inch PVC piping to reduce the transmission of pump-induced vibrations to the test section. Flexible hose segments are incorporated into the loop to further isolate mechanical disturbances and facilitate installation and replacement of the test pipe. Flow rate is regulated using a primary control valve installed along the main line. In addition, a bypass branch redirects a portion of the flow directly back to the reservoir, allowing fine adjustment of operating conditions and improved stability during steady-state measurements. Water was used as the working fluid, with a dynamic viscosity of 0.001 Pa·s and a density of 1000 kg/m³.

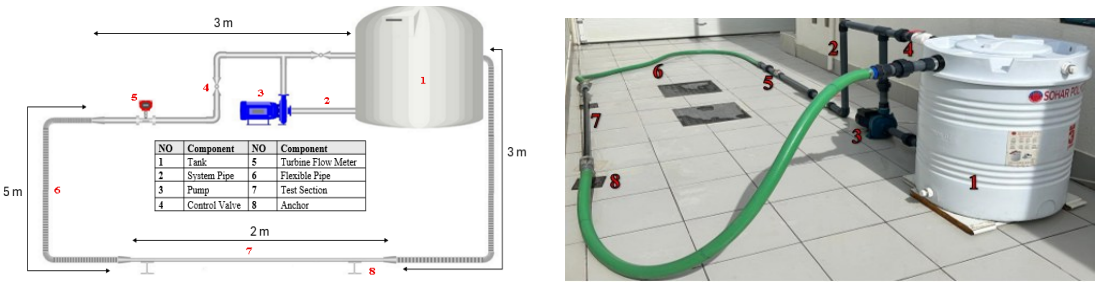

(a) (b)

Figure 1. Experimental setup: (a) Schematic layout, and (b) Actual experimental setup

2.2 Test section

The test section consisted of interchangeable 1-inch Schedule 40 carbon steel (EN 10025 S275JR) and PVC pipes, each 2 m in length, with an outer diameter of 33.4 mm, inner diameter of 26.64 mm, and wall thickness of 3.38 mm. Both pipes were rigidly clamped at both ends to approximate fixed boundary conditions.

2.3 Instrumentation and data acquisition

The reference flow rate was measured using a turbine-type flow meter installed downstream of the flow-control valve. The flow meter operated over a range of 0–700 L/min with a stated accuracy of ±0.5%, providing reliable reference measurements across all operating conditions. Flow-induced vibrations were recorded using a RECOVIB Tiny tri-axial accelerometer mounted at the mid-span of the test pipe. The sensor measured acceleration along three orthogonal axes with a ±15 g range and was connected to a data-acquisition system for continuous recording. Vibration signals were sampled at 1024 Hz per channel with a resolution of 3.66 mg/bit [29].

2.4 Experimental test procedure and repeatability

Experiments were performed outdoors, with fluid temperature assumed to remain within 35–45 °C. Flow rate was regulated using control valves and verified by a turbine flow meter. Carbon-steel tests were conducted from 30 to 230 LPM, and PVC tests from 30 to 210 LPM, both in 20 LPM increments. After each adjustment, the system was allowed to stabilize for approximately 2 min before measurement. Vibration signals were recorded for 90 s using a tri-axial accelerometer mounted at the top mid-span of the test section oriented in three orthogonal directions as illustrated in Figure 2. Each test sequence was repeated ten times to ensure repeatability.

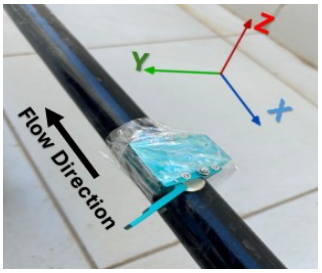

Figure 2. Accelerometer mounting location and orientation

2.5 Data processing methodology

Raw vibration signals were recorded in the time domain and transformed into the frequency domain using the Fast Fourier Transform (FFT). A Strouhal-based estimation was used to identify the

expected range of turbulence-induced excitation frequencies, from which a narrow flow-sensitive frequency band was selected. For each frequency within the selected band, vibration magnitudes in the X, Y, and Z directions were averaged across ten repeated trials for each test case. The trial mean values were then averaged over the entire frequency band to obtain a single representative vibration value for each flow condition and axis. The complete signal processing workflow is illustrated in Figure 3.

Figure 3. Signal processing workflow

2.6 Classical machine learning-based flow estimation

Machine-learning (ML) models were developed to predict flow rates directly from measured tri-axial vibration signals. Features were extracted from the X, Y, and Z-axis data in both the time and frequency domains across six data scenarios (Table 1), including raw and trial-averaged signals, as well as full-spectrum and narrow flow-sensitive frequency bands, where SB denotes the selected flow-sensitive frequency band. In the time domain, model inputs consisted of $X(t)$, $Y(t)$, $Z(t)$, and the corresponding time index t, using either raw signals from all ten trials or signals averaged across trials. In the frequency domain, FFT was applied to obtain 0.5 Hz resolution spectra, where the inputs comprised $X(f)$, $Y(f)$, $Z(f)$, and the frequency index f, again using both raw and average datasets. Additional analyses focused on flow-sensitive frequency regions. No normalization or scaling was applied prior to ML training; all models were trained using vibration amplitudes in their original physical units as obtained from accelerometer measurements and FFT processing. The selected algorithms represent diverse regression strategies. Random Forest (RF), K-Star, Bagging, Decision, and Linear Regression served as a baseline linear model. In addition, Auto-Weka was employed to automate model and hyperparameter optimization using internal cross-validation, ensuring systematic and unbiased model selection. Model performance was evaluated using 10-fold cross-validation and assessed using correlation coefficient (r), mean absolute error (MAE), root mean square error (RMSE), relative absolute error (RAE), and root relative squared error (RRSE).

Table 1. Machine-learning input scenarios used for flow-rate estimation

Scenario	ML input variables	Data description
Raw time-domain	X(t), Y(t), Z(t), t-index	Raw X, Y, Z-axis vibration with time index; 10 full time records for each flow rate
Averaged time-domain	$\bar{X}(t)$, $\bar{Y}(t)$, $\bar{Z}(t)$, t	Mean X, Y, Z-axis vibration from each of the 10 trials at a given flow
Raw full frequency	X(f), Y(f), Z(f), f	X, Y, Z-axis FFT amplitudes with frequency index; full spectrum from 10 trials for each flow rate
Averaged full frequency	$\bar{X}(f)$, $\bar{Y}(f)$, $\bar{Z}(f)$, f	Frequency-domain X, Y, Z-axis vibration with frequency index averaged over 10 trials
Raw sensitive band	X(f), Y(f), Z(f), f within SB	X, Y, Z-axis FFT amplitudes with frequency index inside the sensitive band for all 10 trials
Averaged sensitive band	$\bar{X}(f)$, $\bar{Y}(f)$, $\bar{Z}(f)$, f within SB	Sensitive band X, Y, Z-axis FFT amplitudes with frequency index averaged over 10 trials

2.7 Open loop (series-parallel architecture)

Autoregressive Network with Exogenous Inputs (NARX) was used for training only. In the open-loop (series-parallel) configuration of a NARX or recurrent neural network, the network does not use its own previous predictions as feedback. Instead, it uses the actual measured target values from previous time steps as inputs to the feedback loop. For training purpose, a neural time-series model was employed. In real-world non-intrusive engineering applications, the true flow rate history is unknown; therefore, using the actual measured flow rate from the previous time step as an input is inappropriate. The model should be re-evaluated in "closed-loop mode" (parallel mode), using only the vibration signals and the model's own feedback predictions, to reflect its true predictive capability. In this study, raw vibration signals were used without prior feature reduction. The open-loop network was configured with two input delays, two feedback delays, and ten hidden neurons. Training was conducted in open-loop mode using the Levenberg–Marquardt algorithm to minimize the mean squared error. The dataset was divided into 70% training, 15% validation, and 15% testing subsets. This approach ensures that temporal dependencies are maintained during training and evaluation. Model performance was evaluated using the mean squared error (MSE) and the regression coefficient (R).

3. Results and discussion

3.1 Physical basis for frequency band selection

Measured vibration signals contain contributions from pump excitation, pipe structural response, and flow-induced excitation. Only the flow-induced component varies with flow rate. The centrifugal pump operated at a nominal speed of 2900 rpm, producing a dominant peak at approximately 48.3 Hz, with harmonics at integer multiples. The natural frequencies of the test sections were estimated using the Euler–Bernoulli beam formulation for fixed–fixed boundary conditions [30]. The steel pipe exhibited first-mode frequencies near 43 Hz when filled with fluid, while the PVC pipe was near 9 Hz. Flow-induced excitation frequencies were estimated using the Strouhal number (Eq. (1)) relation [31].

$$f_{\text{peak}} = \frac{St(\text{Re}) \cdot U_c}{D} \tag{1}$$

Where f_{peak} is the characteristic excitation frequency, St is the Strouhal number, Re is Reynolds number Uc is the convective flow velocity, and D is the characteristic diameter (here, pipe inner diameter). In the steel pipe (30–230 LPM), the predicted frequency range spans approximately 4–36 Hz, while for PVC (30–210 LPM) it spans approximately 4–33 Hz. These ranges define the expected flow-sensitive frequency region and remain distinct from pump harmonics and structural resonance.

3.2 Identification of flow-sensitive frequency bands for water in carbon-steel pipe

The vibration response of the 1-inch carbon-steel pipe was analyzed over the frequency range of 4–36 Hz. Frequency-domain spectra were obtained, and the results were averaged across trials to obtain representative vibration amplitudes for each flow rate.

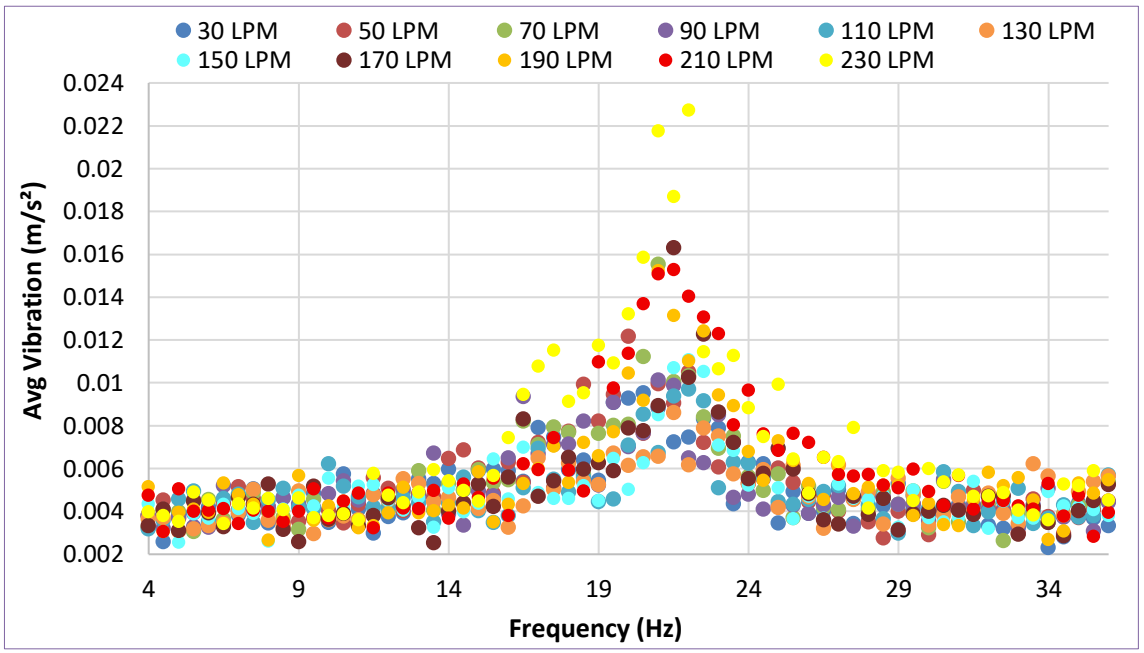

Figure 4. Averaged Z-axis vibration spectra for carbon-steel water flow (4–36 Hz)

Figures 4 and 5 show the averaged vibration spectrum for the Z- and Y-axis components, respectively. Vibration amplitudes remained low below 10 Hz and increased substantially beyond approximately 15 Hz, reaching a clear maximum in the 20–22 Hz range before gradually decreasing toward higher frequencies. This frequency range exhibited the strongest and most consistent dependence on flow rate. The X-axis vibration was excluded due to its low amplitude and weak correlation with flow rate, as axial motion was constrained by the fixed–fixed boundary condition.

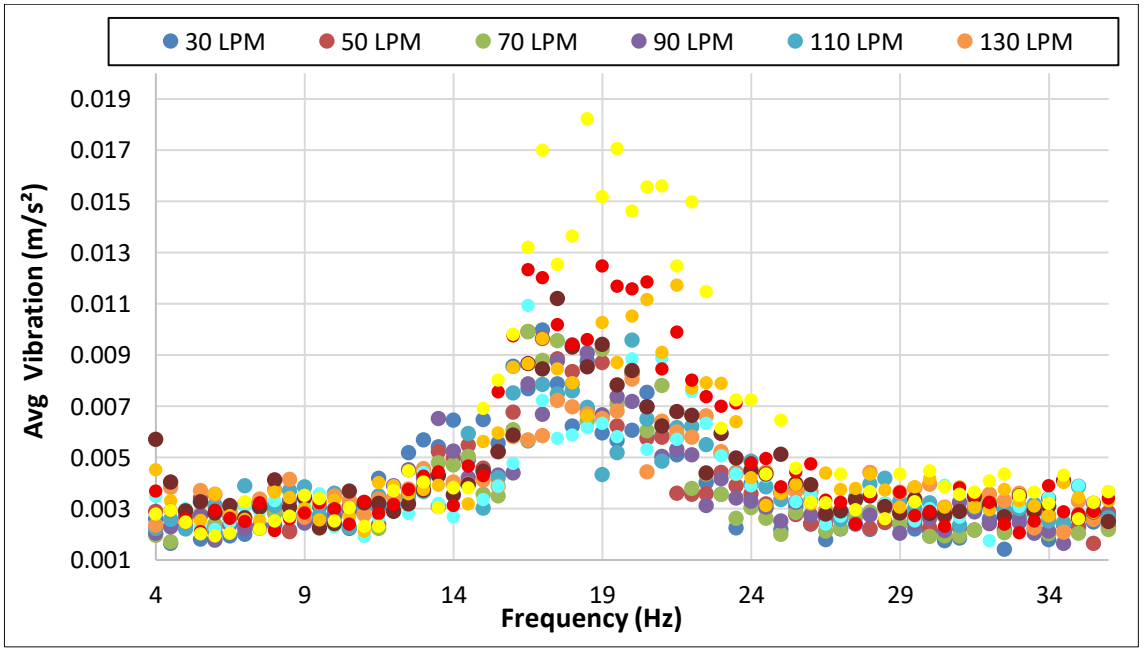

Figure 5. Averaged Y-axis vibration spectra for carbon-steel water flow (4–36 Hz)

Based on the spectral analysis, the 20–22 Hz frequency band was examined in detail for flow sensitivity. For each flow rate between 30 and 230 LPM, FFT magnitudes at 20.0, 20.5, 21.0, 21.5, and 22.0 Hz were averaged across ten trials for the Y- and Z-axis components.

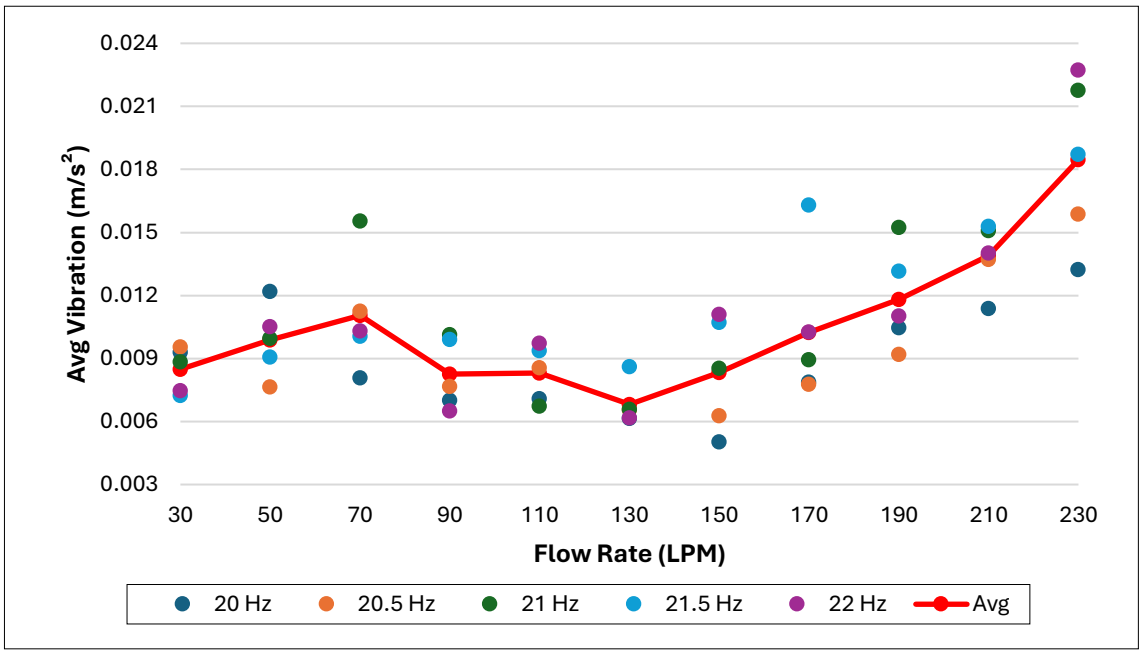

Figure 6. Z Axis-Avg vibrations for 20-22Hz frequencies for carbon-steel water

Figure 6 presents the Z-axis vibration response. Below 130 LPM, the vibration amplitudes exhibit non-monotonic behavior with noticeable changes attributed to flow disturbances from the partially open upstream control valve, which introduce additional local turbulence, resulting in unsteady vibration response at low flow rates. For flow rates above 130 LPM, vibration amplitudes increase monotonically with flow rate across all frequencies. Among the individual frequencies, 21 Hz and 22 Hz show the highest sensitivity and lowest scatter. The band-averaged response (red curve) exhibits a clear increase with flow rate, reaching approximately 0.019 m/s² at 230 LPM. Figure 7 shows the corresponding Y-axis response. Similar trends are observed, although with lower amplitude and greater scatter at low flow rates. Above 130 LPM, the vibration magnitude increases consistently with flow rate across the selected frequency band.

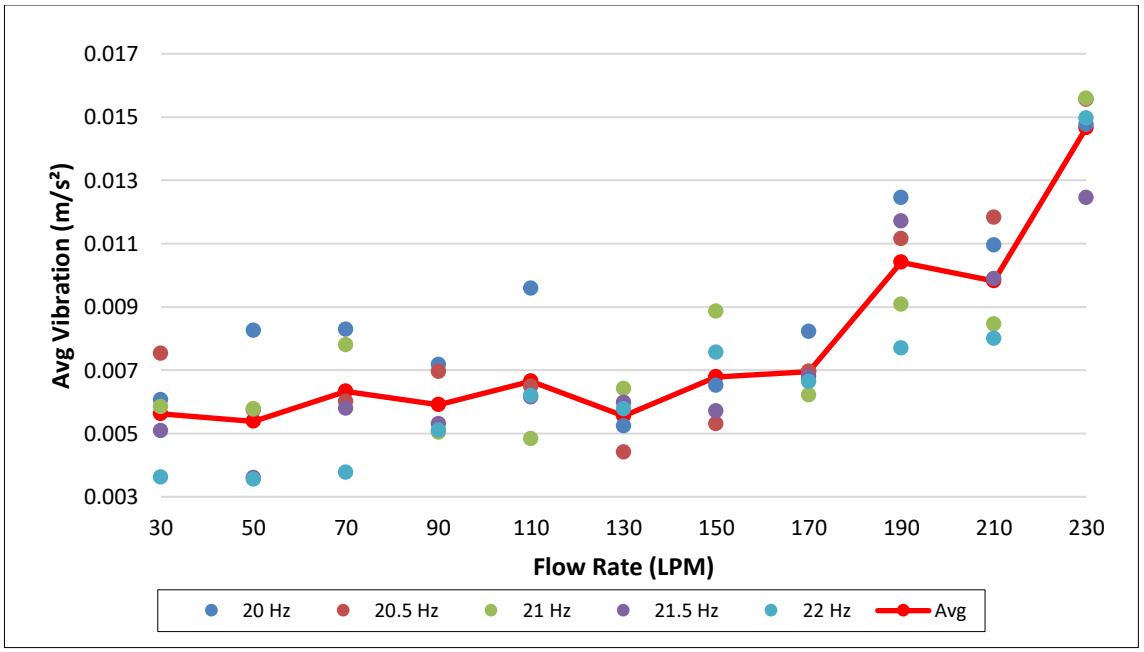

Figure 7. Y Axis-Avg vibrations for 20-22Hz frequencies for carbon-steel water

3.3 Band averaged vibration with trendline for water in carbon-steel pipe

Subsequent analysis focused on the high-flow region between 130 and 230 LPM. For each flow condition, vibration amplitudes in the 20–22 Hz band were averaged to obtain a single representative value per axis. Figure 8 shows the band-averaged vibration magnitude for the Y and Z-axes as a function of flow rate, along with second-order polynomial trendlines. The Z-axis response exhibits a strong and smooth increase with flow rate. The fitted Z polynomial yields an R^2 value of 0.9865, indicating a strong correlation. The Y-axis response exhibits a lower correlation ($R^2 = 0.9141$) and greater scatter.

The second-order polynomial regression models relating vibration amplitude to flow rate are given by Eq. (2) for the Z-axis and Eq. (3) for the Y-axis:

$$V_z = 7.1 \times 10^{-7} Q^2 - 1.4693 \times 10^{-4} Q + 0.01415198 \quad (2)$$

$$V_y = 6.689 \times 10^{-7} Q^2 - 1.579 \times 10^{-4} Q + 0.01500 \quad (3)$$

Where V_z and V_y are the band-averaged vibration amplitudes measured along the Z and Y-axes, respectively, expressed in m/s², and Q is the volumetric flow rate expressed in L/min (LPM).

Model accuracy was evaluated using the percentage error defined in Eq. (4).

$$\text{Percentage Error (\%)} = \left| \frac{V_{\text{actual}} - V_{\text{predicted}}}{V_{\text{actual}}} \right| \times 100 \quad (4)$$

Where V_{actual} and $V_{\text{predicted}}$ represent the actual and model predicted vibration amplitudes, respectively. Z-axis prediction errors remained below 5.4% across the tested range, with a minimum error of 0.39% at 190 LPM. Y-axis errors ranged from 3.5% to 15%, with larger deviations at higher flow rates.

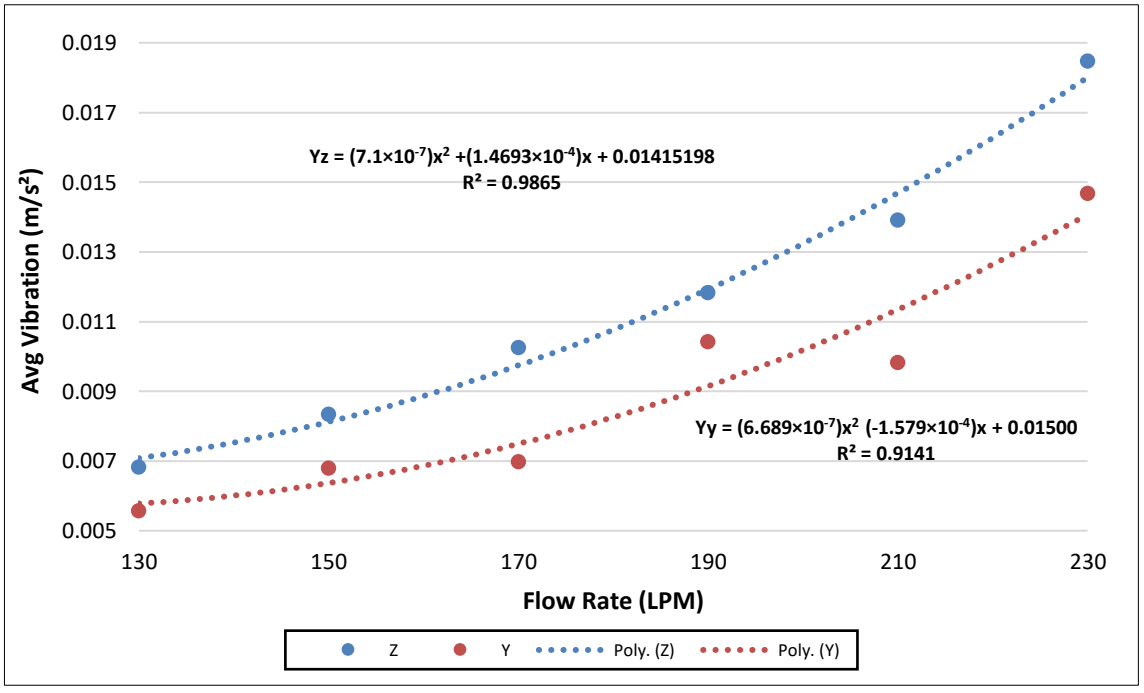

Figure 8. Band-Averaged Z and Y vibrations within 20-22 Hz for carbon-steel water

3.4 Identification of flow-sensitive frequency bands for water in PVC pipe

The vibration response of the 1-inch PVC pipe was analyzed over the frequency range of 4–33 Hz for flow rates between 30 and 210 LPM using trial-averaged FFT spectra from repeated measurements.

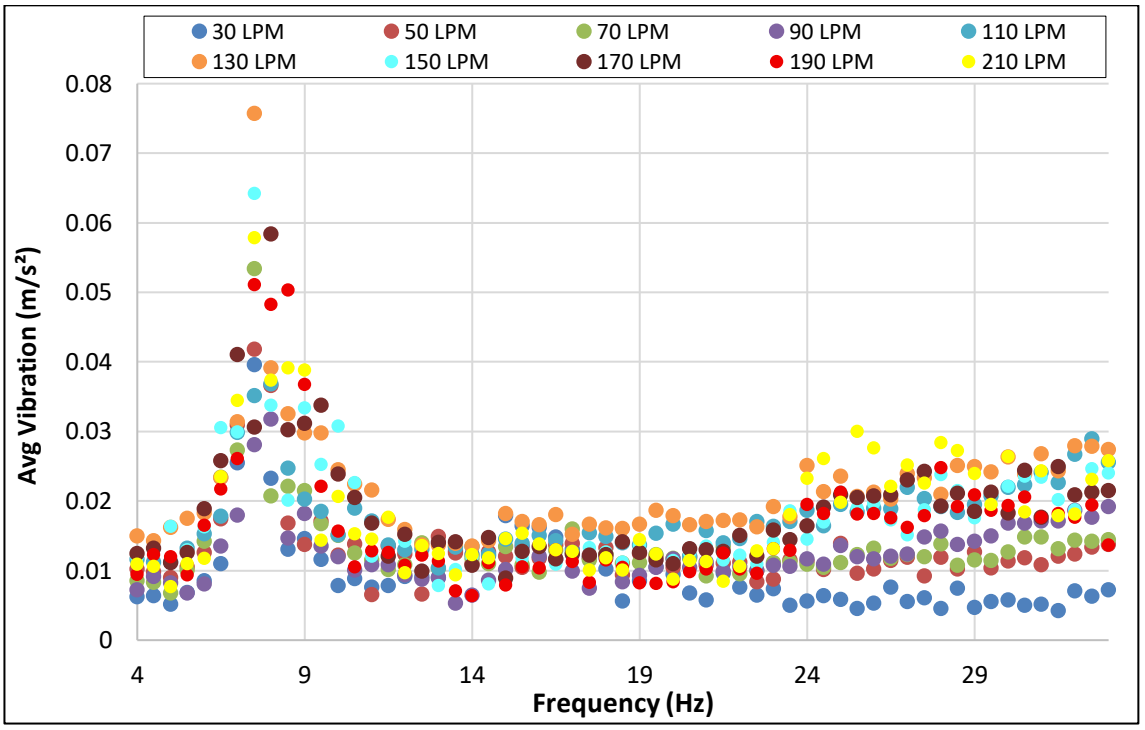

Figure 9. Averaged Z-axis vibration spectra for PVC–water flow (4–33 Hz)

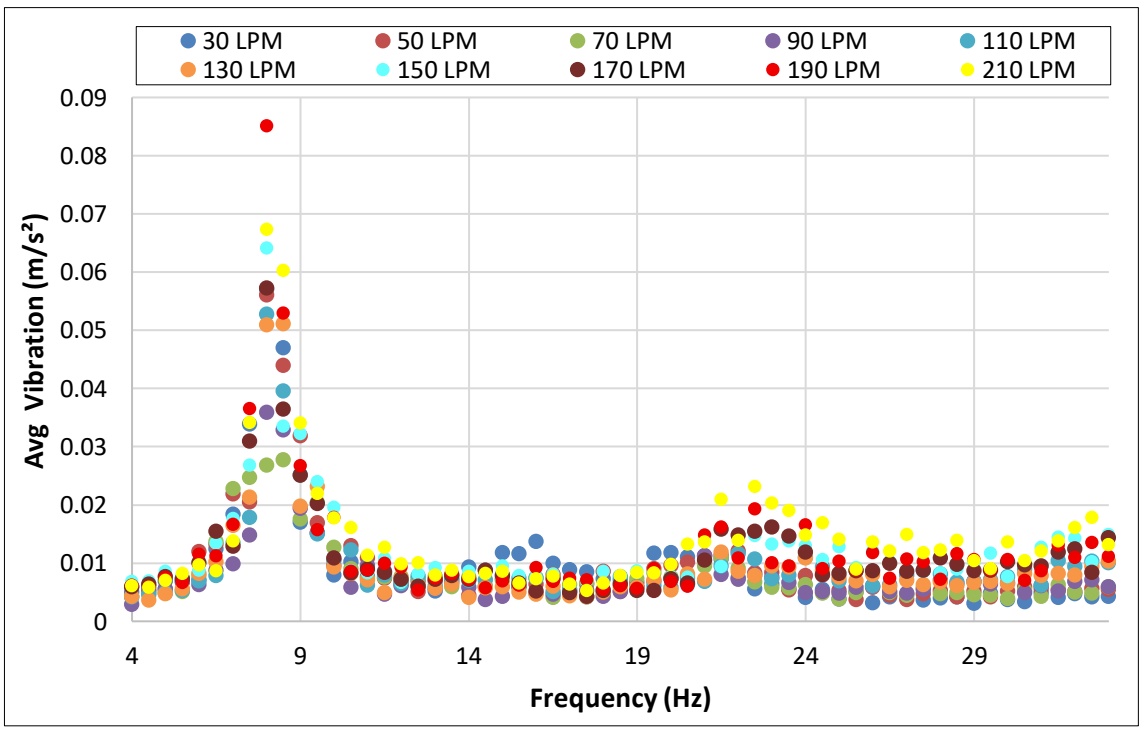

Figure 10. Averaged Y-axis vibration spectra for PVC–water flow (4–33 Hz)

The spectra (Figures 9 and 10) show a dominant resonance peak near 8–9 Hz, corresponding to the first natural frequency of the PVC pipe. This response exhibited high amplitude but weak correlation with flow rate. A second flow-sensitive region was observed at higher frequencies, where vibration amplitude increased consistently with flow rate. Based on this region, refined analysis was performed within the 27.5–29 Hz band for the Z-axis and the 21.5–23 Hz band for the Y-axis. For each flow rate between 30 and 210 LPM, FFT magnitudes at 0.5 Hz intervals were averaged across trials.

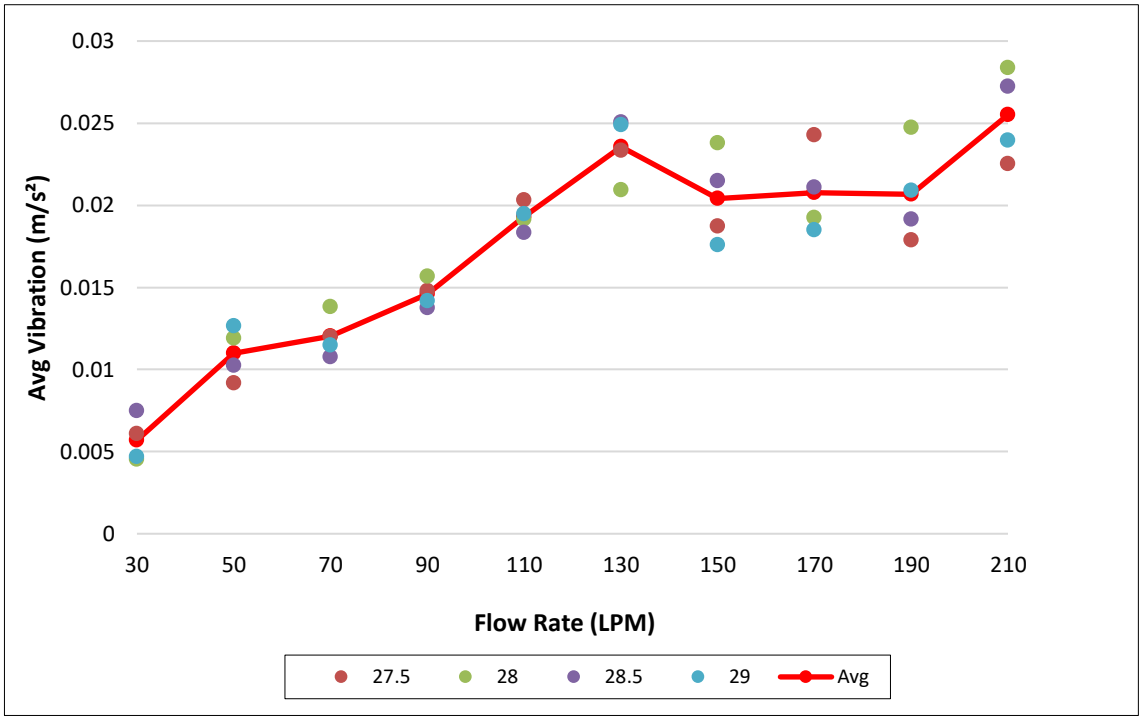

Figure 11. Z Axis-Avg vibrations for 27.5-29 Hz frequencies for PVC–water

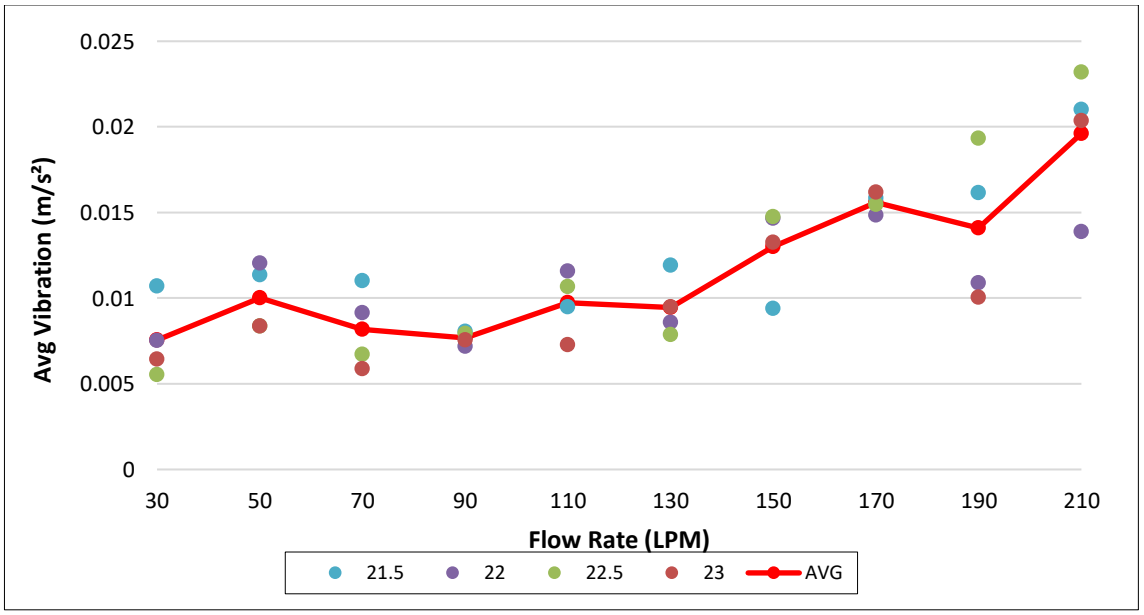

Figure 12. Y Axis-Avg vibrations for 21.5-23 Hz frequencies for PVC–water

Figure 11 shows the Z-axis response over the range 27.5–29 Hz. Vibration amplitudes increase with flow rate, with a local peak near 130 LPM. This peak is attributed to interaction between flow

excitation and the pipe's first natural frequency, followed by a generally increasing trend up to 210 LPM. Figure 12 presents the Y-axis response in the 21.5–23 Hz range, showing a similar but weaker flow-dependent increase, with greater scatter at lower flow rates.

3.5 Band averaged vibration with trendline for water in PVC pipe

For quantitative evaluation, vibration amplitudes within the selected frequency bands were averaged to obtain a single representative value per axis at each flow rate. Figure 13 shows the band-averaged vibration response and corresponding second-order polynomial fits.

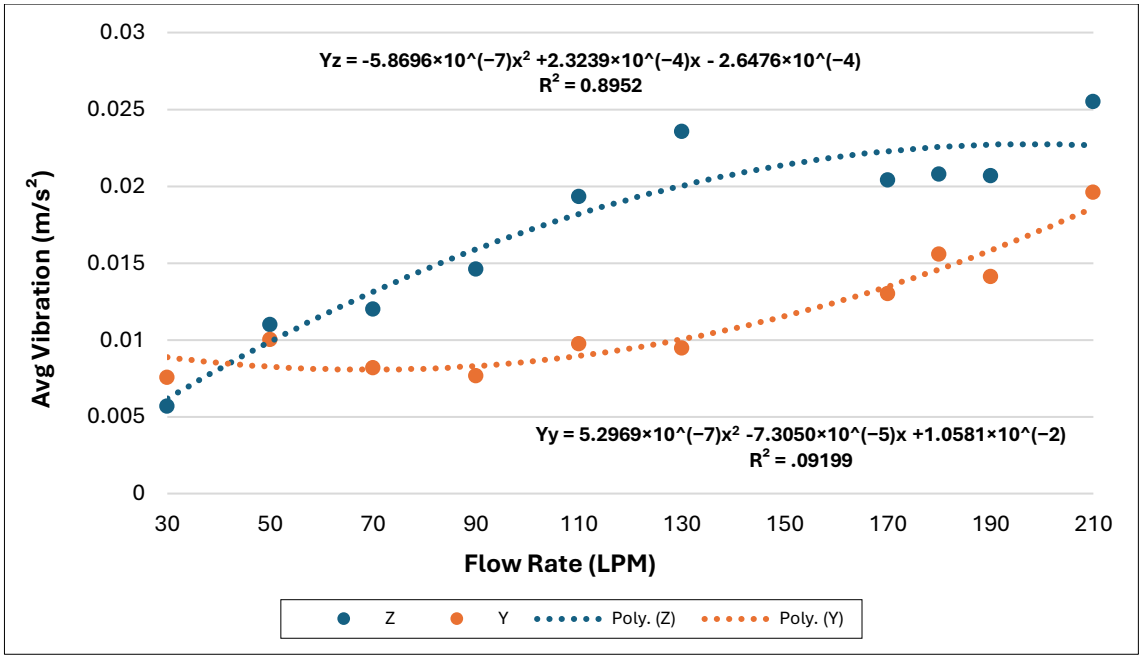

Figure 13. Band-Averaged Z and Y vibrations within 27.5-29 Hz and 21.5-23 Hz, respectively, for PVC–water

The Z-axis band-averaged vibration response shows a clear dependence on flow rate and is described by the second-order polynomial model given in Eq. (5). The fitted model yields a coefficient of determination of $R^2 = 0.8952$, indicating a strong correlation between vibration amplitude and flow rate:

$$V_z = -5.8696 \times 10^{-7} Q^2 + 2.3239 \times 10^{-4} Q - 2.6476 \times 10^{-4} \quad (5)$$

In comparison, the Y-axis vibration amplitudes are lower, the fitted polynomial model yields a slightly higher coefficient of determination ($R^2 = 0.9199$) than that obtained for the Z-axis data. The corresponding second-order polynomial model, given in Eq. (6):

$$V_y = 5.2969 \times 10^{-7} Q^2 - 7.3050 \times 10^{-5} Q + 1.0581 \times 10^{-2} \quad (6)$$

Prediction accuracy was evaluated using the percentage error metric defined previously in Eq. (4). Z-axis errors were generally below 15%, with the maximum deviation occurring near 130 LPM. Y-axis errors ranged between approximately 3% and 17%.

3.6 Comparison between carbon steel and PVC in flow-induced vibrations

The comparison focuses on Z-axis band-averaged vibration amplitudes in the most flow-sensitive frequency bands of 20–22 Hz (carbon steel) and 27.5–29 Hz (PVC). These bands originate from the same flow-induced pressure fluctuations, with minor frequency shifts caused by differences in pipe stiffness, mass, and damping. As shown in Figure 14, both configurations exhibit increasing vibration amplitude with flow rate; however, the PVC pipe consistently produces higher amplitudes due to its lower stiffness and greater wall flexibility. In contrast, the higher rigidity of carbon steel attenuates vibration transmission, resulting in lower response levels.

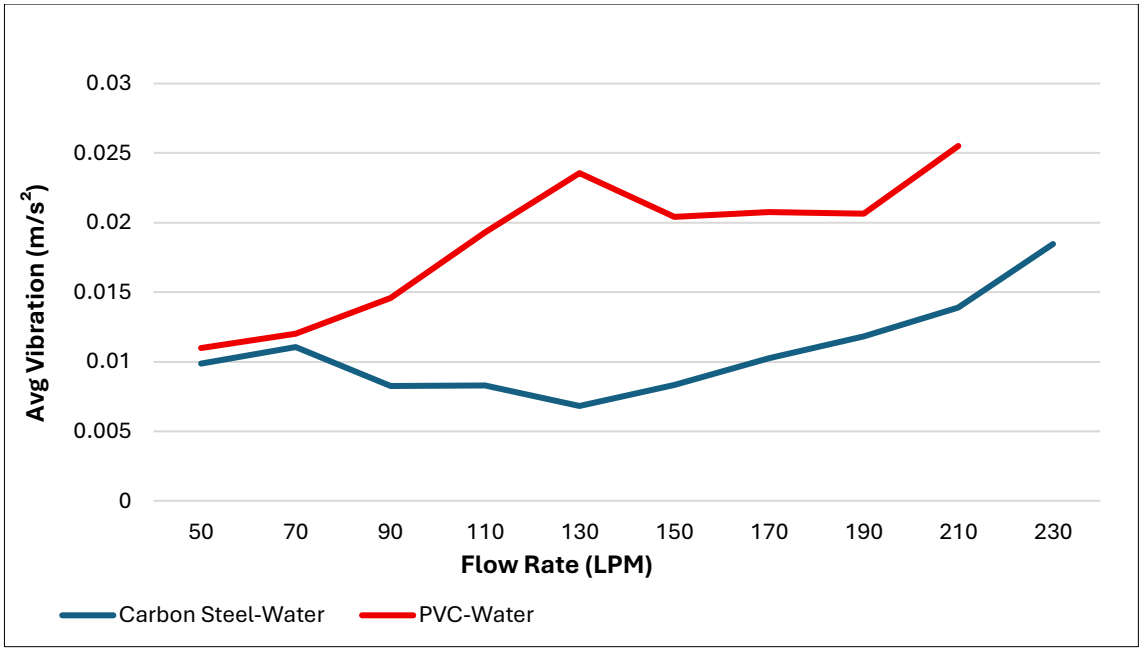

Figure 14. Comparison of average Z-axis band-averaged vibrations of water in carbon steel, and PVC

Following the polynomial fitting analysis, this subsection reports the machine-learning results for the carbon-steel and PVC cases, following the methodology described in Section 2.6. It should be noted that all dataset scenarios were evaluated across all machine-learning algorithms for both pipe materials; however, only the best-performing and most representative results are presented.

3.7 Machine-learning flow estimation results

Following the polynomial fitting analysis, this subsection reports the machine-learning results for the carbon-steel and PVC cases, following the methodology described in Section 2.6. It should be noted that all dataset scenarios were evaluated across all machine-learning algorithms for both pipe materials; however, only the best-performing and most representative results are presented.

3.7.1 Results of machine-learning models for water in a carbon-steel pipe

Machine-learning models were evaluated for the water–carbon steel configuration across six vibration data scenarios. The best-performing results are summarized in Table 2, which also includes the number of instances corresponding to each dataset configuration, providing a clear indication of dataset size and representation. The highest accuracy was obtained using the average time-domain dataset with Auto-WEKA (Random Forest), achieving a correlation coefficient of 0.9167. Averaging reduced random turbulence and sensor noise, allowing the underlying nonlinear relationship between vibration amplitude and flow rate to be captured more effectively. The

averaged frequency-domain dataset (4–36 Hz) produced moderate accuracy (r = 0.6601), as the wide frequency range included components unrelated to flow-induced excitation. The averaged full-spectrum frequency dataset yielded the lowest performance (r = 0.4499), indicating that broadband spectral features mask flow-dependent information in this configuration. Overall prediction accuracy was limited by the low vibration amplitudes. The high stiffness of the steel pipe attenuated flow-induced motion, reducing sensor sensitivity and limiting the ability of the models to capture flow-dependent features.

Table 2. Best-performing machine-learning models for flow rate prediction in the water–carbon steel pipe across different data domains

Dataset	Method	R	MAE (LPM)	RMSE (LPM)	RAE (%)	RRSE (%)	Instances
Averaged time-domain data	Auto-WEKA (RF)	0.9167	20.802	27.873	38.136	44.072	56331
Averaged frequency-domain data (4–36 Hz)	Auto-WEKA (IBk)	0.6601	38.532	47.832	70.641	75.628	715
Averaged full-spectrum frequency data	Bagging	0.4499	45.469	56.645	83.331	89.557	11275

3.7.2 Results of machine-learning models for water in a PVC pipe

The best-performing results are summarized in Table 3. The highest accuracy was achieved using full-spectrum frequency-domain data modeled with Auto-WEKA (Random Forest), yielding a correlation coefficient of 0.9195, and MAE of 18.88 LPM. Averaged full-spectrum data produced nearly identical performance (r = 0.9141), indicating that the vibration response of the PVC pipe is highly repeatable and that averaging provides limited additional benefit.

Table 3. Best-performing machine-learning models for flow-rate estimation in the water–PVC pipe across different data domains

Dataset	Method	r	MAE (LPM)	RMSE (LPM)	RAE (%)	RRSE (%)	Instances
Raw full-spectrum frequency data	Auto-WEKA (RF)	0.9195	18.884	24.798	37.77	43.17	82000
Averaged full-spectrum frequency data	Auto-WEKA (RF)	0.9141	19.821	25.534	39.64	44.45	10250
Averaged time-domain data	Auto-WEKA (RF)	0.8841	21.396	28.297	42.79	49.26	51210
Raw time-domain data	Auto-WEKA (RF)	0.8813	21.398	28.461	42.8	49.54	409680
Averaged frequency-domain data (4–33 Hz)	Auto-WEKA (RF)	0.8574	24.384	32.119	48.77	55.91	590

Time-domain datasets, both raw and averaged, also showed good predictive performance ($r \approx 0.88$), but slightly lower than the frequency-domain cases, as time-domain features capture overall vibration intensity without preserving frequency distribution. The averaged narrowband frequency dataset (4–33 Hz) yielded the lowest accuracy ($r = 0.8574$), indicating that restricting the frequency range excludes relevant flow-dependent components in flexible PVC pipes. The strong performance of full-spectrum frequency features is attributed to the higher vibration amplitudes in PVC. Its lower stiffness enhances wall motion and sensor sensitivity, while simultaneous excitation of multiple modes distributes energy across a wide frequency range, making broadband features highly informative.

3.8 Neural time-series flow estimation training results

The standard industry practice is a two-step hybrid process; training the network in Open Loop where we feed the network historical data and actual targets, so it learns the relationship accurately. Once trained, the second process is transition of the network to a closed-loop mode to perform multi-step predictions into the future where the actual targets are unknown. The NARX open loop raining is highly efficient and much faster. The network prevents cumulative error because it is always "reset" by the correct historical target at every step. The NARX open loop model results are presented here as described in Section 2.7. The regression plots shown in Figures 15 and 16 illustrate excellent training stability. The fitted regression equations, displayed within the figures, provide a quantitative indication of the training accuracy.

For the carbon-steel configuration (Figure 15), the regression lines exhibit slopes very close to unity and minimal intercepts across all datasets, indicating excellent training stability. A slight deviation from the ideal line is observed in the test dataset, with marginal underestimation present at higher flow rates. Nevertheless, the high correlation coefficient ($R \approx 1.0$) and low validation mean squared error (MSE = 0.0110) confirm that the NARX model effectively trains the nonlinear relationship between flow rate and vibration response.

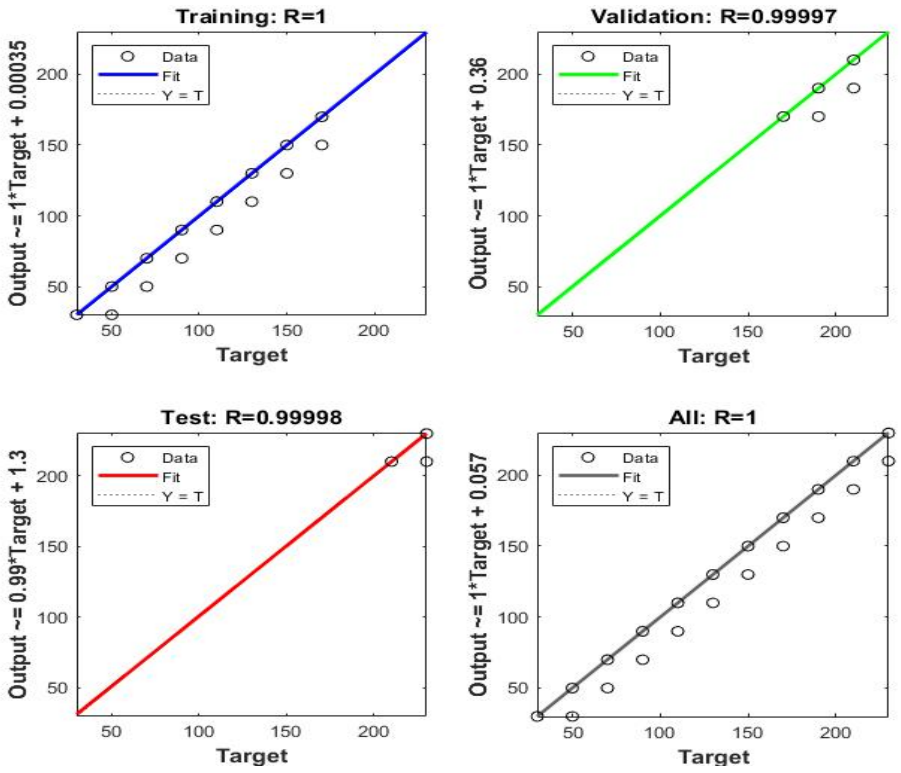

Figure 15. Regression results of the open-loop NARX model for water–carbon steel (Training stage only)

A similar trend is observed for the PVC configuration (Figure 16), where the regression lines also closely follow the ideal unity relationship, with small intercepts indicating minimal prediction bias. The model achieves a slightly lower validation MSE (0.00981), reflecting improved predictive performance compared to the carbon-steel case. This improvement can be attributed to the higher vibration amplitudes observed in the PVC pipe due to its lower structural stiffness, which enhances the signal-to-noise ratio and provides clearer dynamic patterns for the model to learn. Overall, the NARX model demonstrates strong capability in training the dynamic and nonlinear characteristics of flow-induced vibrations for both pipe materials.

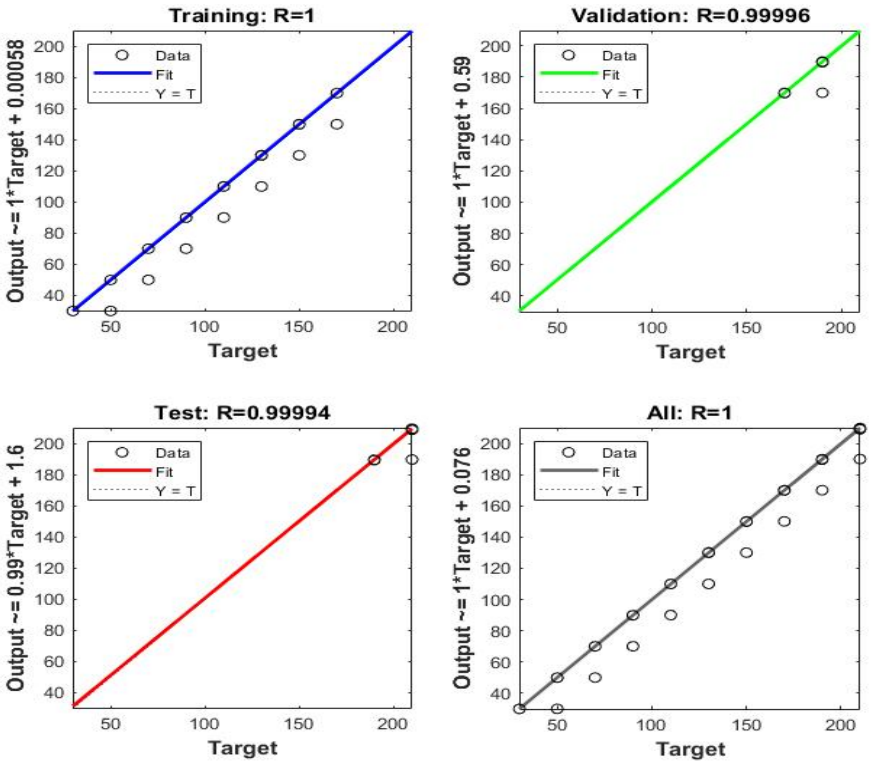

Figure 16. Regression results of the open-loop NARX model for water PVC (Training stage only)

3.9 Discussion of results

Previous studies have consistently reported strong relationships between vibration features and flow rate. For example, [17], [14], and [19] observed linear or quadratic trends for water flow, with correlation coefficients ranging from $R^2 = 0.978$ to 0.997. The present study shows comparable behavior, achieving $R^2 = 0.9865$ for carbon steel and approximately $R^2 \approx 0.90$ for PVC. This agreement confirms the consistency of vibration-based flow relationships across different sensing techniques and pipe configurations. The slight reduction in accuracy for PVC suggests that material-dependent effects influence the stability of the vibration response.

The influence of pipe material observed in this study is consistent with findings reported by [10], [13], who showed that flexible materials such as PVC exhibit higher vibration amplitudes and greater variability due to lower stiffness, while denser materials damp vibrations more effectively. In the present work, the PVC pipe exhibited greater scatter and larger prediction errors than carbon steel, which can be attributed to its lower structural stiffness and higher sensitivity to turbulence-induced excitation.

In terms of modeling approaches [12] demonstrated the effectiveness of neural network models for vibration-based flow estimation, achieving low RMS errors using time-domain data in steel pipes. Classical machine-learning models achieved strong predictive performance across different data

scenarios, with correlation coefficients reaching approximately $R \approx 0.92$. It was observed that more data scenarios yielded stronger predictive performance in the PVC case than in the carbon steel case. This behavior is attributed to the higher vibration amplitudes in PVC, which enhance signal clarity and improve the model's ability to learn relevant patterns.

Neural time-series modeling in open-loop mode is acceptable and commonly used for training purposes because it facilitates stable and efficient learning. Performance evaluation should be conducted in closed-loop mode to reflect realistic operating conditions. Evaluating the model using actual previous target values provides optimistic accuracy estimates and does not demonstrate the model's ability to perform autonomous multi-step prediction in practical applications where the true output history is unavailable. Furthermore, the NARX neural network demonstrated excellent capability in training the dynamic behavior of flow-induced vibrations, achieving validation MSE values below 0.01 and correlation coefficients of $R \approx 1.0$. Models dynamically transition through a two-step process to optimize performance. In real applications, we first train the network using the stable series-parallel (open-loop) architecture, then switch to a parallel (closed-loop) architecture for multi-step predictions or system estimation. The latter model was not implemented in this work.

4. Conclusion

This study demonstrated the feasibility of using flow-induced vibrations (FIV) for non-intrusive flow-rate estimation in both PVC and carbon-steel pipes. Band-averaged vibration amplitudes generally increased with flow rate within material-dependent frequency bands, with the Z-axis providing the highest sensitivity. PVC exhibited higher vibration amplitudes than carbon steel due to lower stiffness. A comparative evaluation of analytical and data-driven approaches showed that frequency-band analysis and polynomial regression provide clear physical interpretation and strong predictive performance ($R^2 \approx 0.99$ for carbon steel and $R^2 \approx 0.90$ for PVC), but are limited in capturing nonlinear behavior across broader operating conditions. Classical machine-learning models improve flexibility and generalization, achieving consistent performance ($R \approx 0.92$), with a broader range of data scenarios, achieving strong performance in PVC due to higher signal amplitudes and improved feature separability. open-loop (series-parallel) architecture, which was carried in this work, is the standard and recommended way to initially train and develop the closed-loop (parallel) network. Future work is to convert the network into a closed-loop (parallel) architecture, where it feeds its own predicted outputs back into the input layer for multi-step-ahead forecasting. Future work should also focus on improving model generalization, extending validation across different fluids and pipeline conditions, and developing real-time implementation strategies for practical deployment.

Author's declaration

Author contribution

Khalid Alnabhani: Conceptualization, Methodology, Software, Validation, Formal analysis, Investigation, Data curation, Visualization, Writing-original draft preparation, and Writing-review and editing. **Musaab Zarog:** Conceptualization, Supervision, Validation, Project administration, Resources, and Review and editing. **Hadj Bourdoucen:** Project administration, and Resources.

Funding statement

This work was funded by the Sultan Qaboos University-Qatar University joint grant No. CL/SQU\QU/ENG/24/01.

Data availability

The data supporting the findings of this study are available from the corresponding author upon reasonable request. The data are not publicly available due to ongoing analysis and use in related research projects.

Acknowledgements

The authors would like to acknowledge Sultan Qaboos University for providing the laboratory facilities, technical resources, and research environment that supported the experimental work conducted in this study.

Competing interest

The authors declare that they have no known competing financial interests or personal relationships that could have appeared to influence the work reported in this paper.

Ethical clearance

Not Applicable.

AI statement

ChatGPT was used only for grammar and language refinement. All scientific content and interpretations are the original work of the authors. Furthermore, this manuscript has been comprehensively proofread by an English language expert to ensure linguistic accuracy and clarity. The author reviewed and verified all scientific content and takes full responsibility for the manuscript.

Publisher's and Journal's note

Universitas Negeri Padang as the publisher, and Editor of Teknomekanik state that there is no conflict of interest towards this article publication.

References

[1] M. Pereira, "Flow meters: Part 1," *Instrumentation & Measurement Magazine, IEEE*, vol. 12, pp. 18–26, Dec. 2009, https://doi.org/10.1109/MIM.2009.4762948

[2] P. Mohindru, "Recent advancements in volumetric flow meter for industrial application," *Heat and Mass Transfer*, vol. 59, pp. 1–18, May 2023, https://doi.org/10.1007/s00231-023-03413-4

[3] R. C. . Baker, *Flow measurement handbook : industrial designs, operating principles, performance, and applications*. Cambridge University Press, 2000.

[4] M. Al Sawwafi, M. Zarog, R. Zaier, and A. Al Yahmedi, "Modeling Flow-Induced Vibration of Pipes in Oil Industry: A Case Study," *Romanian Journal of Acoustics and Vibration*, vol. 22, pp. 111–115, Dec. 2025. https://rjav.sra.ro/index.php/rjav/article/view/449

[5] F. Villa, C. Sánchez, M. Vallejo, J. S. Botero-Valencia, and E. Delgado-Trejos, "Dataset of Flow-Induced Vibrations on a Pipe Conveying Cold Water," *Data (Basel).*, vol. 6, no. 9, 2021, https://doi.org/10.3390/data6090100

[6] J. Wang, S. Li, and C. Bose, "Effect of a fixed downstream cylinder on the flow-induced vibration of an elastically supported primary cylinder," *Physics of Fluids*, vol. 36, May 2024, https://doi.org/10.1063/5.0207136

[7] X. Fu, S. Fu, N. Zhibo, B. Zhao, J. Shen, and P. Deng, "A validated fluid-structure interaction simulation model for vortex-induced vibration of a flexible pipe in steady flow." May 2025. https://doi.org/10.48550/arXiv.2502.05748

[8] M. I. Mohd Ismail *et al.*, "A review of vibration detection methods using accelerometer sensors for water pipeline leakage," *IEEE Access*, vol. 7. Institute of Electrical and Electronics Engineers Inc., pp. 51965–51981, 2019. https://doi.org/10.1109/ACCESS.2019.2896302

[9] J. Shen *et al.*, "Experimental Investigation on Vortex Induced Vibration of a Rigidly Coupled Twin-Tube Model," May 2024. https://doi.org/10.1115/OMAE2024-122890

[10] R. P. Evans, J. D. Blotter, and A. G. Stephens, "Flow rate measurements using flow-induced pipe vibration," in *Journal of Fluids Engineering, Transactions of the ASME*, Mar. 2004, pp. 280–285. https://doi.org/10.1115/1.1667882

[11] J. E. Urrea, L. E. Escobar-Correa, J. P. Morán-Zabala, A. F. Ramirez-Barrera, J. I. Padilla-Buritica, and E. Delgado-Trejos, "Flow rate estimation from flow-induced vibration using signal decomposition and advanced regression models," *Flow Measurement and Instrumentation*, vol. 107, p. 103084, 2026, https://doi.org/https://doi.org/10.1016/j.flowmeasinst.2025.103084

[12] S. K. Venkata and B. R. Navada, "Estimation of flow rate through analysis of pipe vibration," *Acta Mechanica et Automatica*, vol. 12, no. 4, pp. 294–300, Dec. 2018, https://doi.org/10.2478/ama-2018-0045

[13] M. T. Pittard, R. P. Evans, R. D. Maynes, and J. D. Blotter, "Experimental and numerical investigation of turbulent flow induced pipe vibration in fully developed flow," *Review of Scientific Instruments*, vol. 75, no. 7, pp. 2393–2401, Jul. 2004, https://doi.org/10.1063/1.1763256

[14] G. Dinardo, L. Fabbiano, and G. Vacca, "Fluid flow rate estimation using acceleration sensors," in *Proceedings of the International Conference on Sensing Technology, ICST*, 2013, pp. 221–225. https://doi.org/10.1109/ICSensT.2013.6727646

[15] S. Chun, S. Lee, and H. Yoon, "Use of Laser Doppler Vibrometry for Measuring Flow-Induced Vibration of a Thermowell in a Pipe Flow," May 2021. https://doi.org/10.1115/FEDSM2021-64609

[16] M. M. Campagna, G. Dinardo, L. Fabbiano, and G. Vacca, "Fluid flow measurements by means of vibration monitoring," *Meas. Sci. Technol.*, vol. 26, no. 11, Oct. 2015, https://doi.org/10.1088/0957-0233/26/11/115306

[17] K. A. R. Medeiros, C. R. H. Barbosa, and E. C. De Oliveira, "Flow measurement by piezoelectric accelerometers: Application in the oil industry," *Pet. Sci. Technol.*, vol. 33, no. 13–14, pp. 1402–1409, 2015, https://doi.org/10.1080/10916466.2015.1044613

[18] S A. Awawdeh, S. T. S. Bukkapatnam, S. R. T. Kumara, C. Bunting, and R. Komanduri, "Wireless sensing of flow-induced vibrations for pipeline integrity monitoring," in Fourth *IEEE Workshop on Sensor Array and Multichannel Processing*, 2006., 2006, pp. 114–117. https://doi.org/10.1109/SAM.2006.1706103

[19] Y. Shang, C. Wang, Y. Zhang, W. Zhao, J. Ni, and G. Peng, "Non-Intrusive Pipeline Flow Detection Based on Distributed Fiber Turbulent Vibration Sensing," *Sensors*, vol. 22, no. 11, Jun. 2022, https://doi.org/10.3390/s22114044

[20] S. Wang, D. Xu, G. Liu, T. Xue, and Y. Liu, "Application of Distributed Acoustic Sensing Technology in Pipeline Leakage Monitoring," *Journal of Energy and Natural Resources*, vol. 13, pp. 81–89, May 2024, https://doi.org/10.11648/j.jenr.20241302.14

[21] H. Ding and J. C. Ji, "Vibration control of fluid-conveying pipes: a state-of-the-art review," *Applied Mathematics and Mechanics (English Edition)*, vol. 44, pp. 1423–1456, Sep. 2023, https://doi.org/10.1007/s10483-023-3023-9

[22] M. H. Bin Abdul Hamid, "Experimental study on pipe fluid induced vibration," Universiti Teknologi PETRONAS, Tronoh (MY), 2013. https://utpedia.utp.edu.my/id/eprint/10608/1/Dissertation%20Report_14593.pdf

[23] S. M. Khot, P. Khaire and A. S. Naik, "Experimental and simulation study of flow induced vibration through straight pipes," 2017 *International Conference on Nascent Technologies in*

Engineering (ICNTE), Vashi, India, 2017, pp. 1-6. https://doi.org/10.1109/ICNTE.2017.7947938

[24] Y.-J. Cha, R. Ali, J. Lewis, and O. Büyüköztürk, "Deep learning-based structural health monitoring," *Autom. Constr.*, vol. 161, p. 105328, 2024, https://doi.org/https://doi.org/10.1016/j.autcon.2024.105328

[25] O. Matania, I. Dattner, J. Bortman, R. S. Kenett, and Y. Parmet, "A systematic literature review of deep learning for vibration-based fault diagnosis of critical rotating machinery: Limitations and challenges," *J. Sound Vib.*, vol. 590, p. 118562, 2024, https://doi.org/https://doi.org/10.1016/j.jsv.2024.118562

[26] B. A. Tama, M. Vania, S. Lee, and S. Lim, "Recent advances in the application of deep learning for fault diagnosis of rotating machinery using vibration signals," *Artif. Intell. Rev.*, vol. 56, no. 5, pp. 4667–4709, 2023, https://doi.org/10.1007/s10462-022-10293-3

[27] F. Saleem, Z. Ahmad, and J.-M. Kim, "Real-Time Pipeline Leak Detection: A Hybrid Deep Learning Approach Using Acoustic Emission Signals," *Applied Sciences*, vol. 15, no. 1, 2025, https://doi.org/10.3390/app15010185

[28] S. Heydari, R. Gao, and R. K. Jaiman, "Predicting flow-induced vibration in isolated and tandem cylinders using hypergraph neural networks," *Comput. Fluids*, vol. 307, p. 106930, 2026, https://doi.org/https://doi.org/10.1016/j.compfluid.2025.106930

[29] "RECOVIB® Tiny by Micromega Dynamics." Accessed: Nov. 16, 2024. [Online]. Available: https://micromega-dynamics.com/products/recovib/miniature-vibration-recorder/

[30] L. Meirovitch, *Elements of Vibration Analysis*, 2nd ed. New York: McGraw-Hill, 1986.

[31] R. D. Blevins, *Flow-Induced Vibration*, 2nd ed. New York: Van Nostrand Reinhold, 1990.

Nomenclature

D	Pipe inner diameter (m)
DAS	Distributed Acoustic Sensing
FFT	Fast Fourier transform
FIV	Flow-induced vibration
LES	Large Eddy Simulation
LVD	Laser Doppler Vibrometer
MAE	Mean absolute error
MSE	Mean square error
NARX	Nonlinear autoregressive model with exogenous input
PVC	Polyvinyl chloride
Q	Flow rate (LPM)
R, r	Correlation coefficient
R^2	Coefficient of determination
RAE	Relative absolute error
Re	Reynolds number
RMSE	Root mean square error
RRSE	Root relative squared error
St	Strouhal number
U_c	Convection velocity (m/s)
V_{actual}	Actual model vibration amplitude (m/s²)
V_{pred}	Predicted model vibration amplitude (m/s²)
V_y	Band average vibration amplitude in y-direction (m/s²)
V_z	Band average Vibration amplitude in z-direction (m/s²)
f_{peak}	Peak vibration frequency (Hz)